

Heterogeneous Reactions of Glyoxal on Particulate Matter: Identification of Acetals and Sulfate Esters

JOHN LIGGIO,[†] SHAO-MENG LI,[‡] AND ROBERT MCLAREN^{*,†}

Centre for Atmospheric Chemistry and Chemistry Department, York University, 4700 Keele Street, Toronto, Ontario, M3J 1P3 Canada, and Meteorological Service of Canada, 4905 Dufferin Street, Toronto, Ontario, M3H 5T4 Canada

Reactive uptake of glyoxal onto particulate matter has been studied in laboratory experiments in a 2 m³ Teflon reaction chamber. Inorganic seed particles of different composition were utilized, including (NH₄)₂SO₄, (NH₄)₂SO₄/H₂SO₄, NaNO₃, and simulated sea salt, while the relative humidity and acid concentration were varied. The organic composition of the growing particles was measured in situ with an aerosol mass spectrometer, providing particle mass spectra as a means of product identification. Aerosol physical characteristics were also measured with a differential mobility analyzer and condensation nucleus counter. Regardless of seed composition, particle growth was rapid and continuous over the course of several hours. Identification of several mass fragments greater than the glyoxal monomer suggested that heterogeneous reactions to form glyoxal adducts of low volatility had occurred. Temporal analysis of the mass fragments was consistent with a proposed acid-catalyzed mechanism whereby glyoxal is first hydrated, followed by self-reaction to form cyclic acetal structures. Increased relative humidity slowed the formation of higher order oligomers, also consistent with the proposed mechanism. The relative contribution of various oligomers to the overall organic composition was strongly dependent on the relative humidity and hence the particulate water concentration. A mild acid catalysis was also observed upon increasing the acidity of the seed particles. Specific mass fragments were found that could only arise from sulfate esters and were not present on the non-sulfur-containing seed particles. This first evidence of the formation of organic sulfates in particles is presented together with a proposed mechanism and molecular structure. These results suggest that the formation of these products of glyoxal uptake can contribute significantly to secondary organic aerosol.

Introduction

The focus of atmospheric chemistry is shifting toward the study of secondary organic aerosol (SOA) formation via gas–particle partitioning processes. An understanding of these processes is important because aerosols play a role in climate change (1, 2) and visibility (3–5). Also, studies have demonstrated that particles, particularly those containing organic species, can cause adverse health effects (6–8). Much of the

study with respect to SOA focuses on low-volatility products, which are expected to easily partition into the particle phase. This expectation is rooted in existing gas–particle partitioning theory, based on the vapor pressure of the species in question (9–12). However, deviations from partitioning theory for volatile and semivolatile products of toluene and α -pinene photooxidation have been reported (13, 14). In particular, aldehydes and ketones can contribute significantly to this deviation. Although the role of gas-phase carbonyls as a source of radicals (15) and organic nitrates (16, 17) has been studied extensively, little is known regarding their contribution to SOA by means of heterogeneous reactions. Recent work has suggested that additional partitioning of carbonyls to particulate material may occur via chemical transformation of the carbonyl to low-volatility products in the aerosol (18–23). One potential mechanism for this involves the hydration of the carbonyl followed by acid-catalyzed polymerization or acetal/hemiacetal formation in the presence of alcohols (20–22). Aldol condensation (23) and other reactions known to occur in bulk solution have also been postulated as a means of forming low-volatility products in aerosols (18, 19). Heterogeneous reactions of these types imply that SOA yields may be significantly larger than those predicted by partitioning theory, which is especially relevant given that most organic photooxidation products contain carbonyl functionality.

The dialdehyde glyoxal is one of several dicarbonyl species that are formed in significant yields from the photooxidation of aromatic hydrocarbons (13, 24–27). It has also been identified as a minor oxidation product of isoprene (15, 28–30), as well as other biogenic species (31). Given the varied sources of glyoxal and the prevalence of aromatic and biogenic species in ambient air, partitioning of glyoxal could be a significant contributor to SOA, particularly in light of potential heterogeneous reactions that have been proposed (22). Glyoxal is an excellent candidate for studying such reactions because it is significantly more reactive with respect to hydration, polymerization, and hemiacetal formation than most other aldehydes. Also, the relatively simple structure of glyoxal precludes an aldol condensation mechanism from occurring, thereby reducing the complexity of observed reaction products. In fact, glyoxal has been found to produce significant aerosol yields, attributed to hydration and polymerization (22). Much of the structural evidence supporting these mechanisms has typically relied on optical methods to determine the functionality of the resultant particulate products, specifically the C–O–C bond stretch (20–22). Only recently has mass spectral evidence begun to appear for hydration and polymerization of products derived from the photooxidation of α -pinene (20); however, the exact structure of the glyoxal reaction products and thus the heterogeneous reaction mechanism remains undetermined. Although formation of glyoxal–sulfite adducts has been reported as a possible heterogeneous reaction mechanism (18), the potential formation of carbonyl sulfates on sulfate-containing aerosols has not been studied. This can occur via an esterification reaction as an alternative to, or simultaneously with, other polymerization or acetal formation mechanisms.

In the present work, gaseous glyoxal was exposed to several types of seed aerosols under different conditions within an enclosed chamber while an aerosol mass spectrometer (AMS) was used to probe the chemical composition of glyoxal in the growing particles. Particle mass spectra were obtained on-line during reactive uptake. The use of the AMS in conjunction with differing seed particles provides insight into the heterogeneous reactions that occur during the uptake. Possible structures and mechanisms for hydration

* Corresponding author phone: (416)736-2100, ext 30675; fax: (416)736-5936; e-mail: rmclaren@yorku.ca.

[†] York University

[‡] Meteorological Service of Canada.

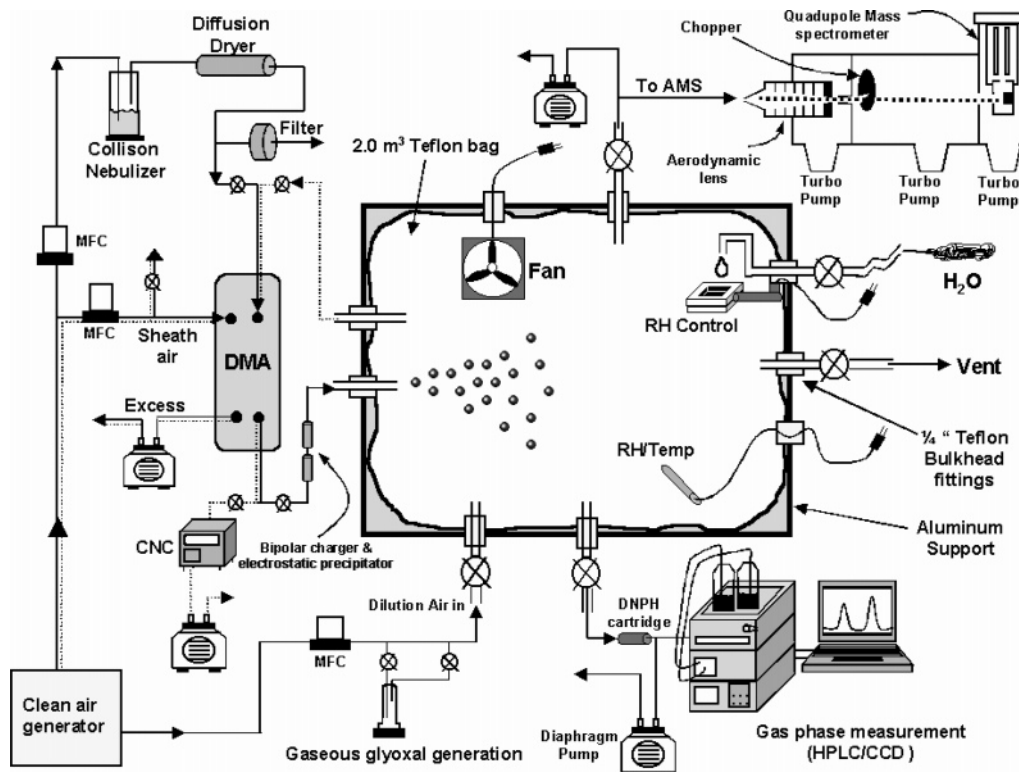


FIGURE 1. Schematic representation of experimental system. Dashed lines represent DMA/CNC sampling mode of operation. Solid lines represent the filling mode of operation.

and acetal formation of glyoxal are presented. In addition, preliminary evidence is presented for the formation of glyoxal sulfates that appears to occur simultaneously.

Experimental Procedures

Overview. The apparatus utilized in these experiments is given schematically in Figure 1. Studies were conducted in a 2 m³ Teflon bag (Welch Fluorocarbon Inc.) enclosed in an aluminum support to exclude any photochemistry. Particles of known inorganic composition were introduced into the bag with preexisting gaseous glyoxal. Particle growth was monitored with a scanning differential mobility analyzer (DMA) and condensation nuclei counter (CNC) as well as an aerosol mass spectrometer (AMS, Aerodyne Research Inc.). Mass spectra of an ensemble of particles were obtained with the AMS that provided structural information for the organics and time-dependent size distributions. A hygrometer probe

inside the chamber monitored the temperature and relative humidity, while a fan with a volumetric flow rate of approximately 1 m³/min ensured adequate mixing. The temperature remained approximately constant at 25 °C. The relative humidity was controlled by manually injecting liquid water onto a temperature-controlled, resistively heated element that completely vaporized the water. In this manner, a relative humidity of 5–100% within the bag could be achieved in less than 5 min. Particle- and organic-free air (Aadco) was used as dilution air for all experiments.

Particle Generation. Atomizing appropriate aqueous solutions with a collision nebulizer (BGI Inc.) generated particles of different chemical composition. A list of the solutions used and other experimental conditions is given in Table 1. The DMA/CNC was used to both size-select the particles introduced into the chamber (filling mode) and to

TABLE 1. Summary of the Conditions and Duration of Glyoxal Uptake Experiments

expt	seed type	nebulizer solution ^a (M)	RH (%)	initial seed	particle filling time (min)	gaseous glyoxal (ppb)	total exposure time (min)
1	(NH ₄) ₂ SO ₄	SO ₄ ²⁻ = 0.024, NH ₄ ⁺ = 0.048, H ₃ O ⁺ = 5 × 10 ⁻⁶	49	wet	97	5.1	235
2	<i>b</i>	<i>b</i>	98	wet	60	4.8	245
3	(NH ₄) ₂ SO ₄ /H ₂ SO ₄	HSO ₄ ⁻ = 0.033, SO ₄ ²⁻ = 0.029, H ₃ O ⁺ = 0.042, NH ₄ ⁺ = 0.048	55	wet	48	4.8	252
4	<i>b</i>	<i>b</i>	98	wet	48	3.6	186
5	<i>b</i>	<i>b</i>	11	dry	48	4.8	114
6	(NH ₄) ₂ SO ₄ /H ₂ SO ₄	HSO ₄ ⁻ = 0.096, SO ₄ ²⁻ = 0.042, H ₃ O ⁺ = 0.130, NH ₄ ⁺ = 0.050	50	wet	60	4.5	174
7	<i>b</i>	<i>b</i>	88	wet	48	5.3	144
8	simulated sea salt	NaCl = 4.63 × 10 ⁻³ , KCl = 1.14 × 10 ⁻³ , MgCl ₂ = 7.5 × 10 ⁻³ , CaCl ₂ = 1.1 × 10 ⁻³	70	wet	60	4.9	120
9	NaNO ₃	NaNO ₃ = 0.038	60	wet	66	5.4	126
10	NaNO ₃ /HNO ₃	NO ₃ ⁻ = 0.060, Na ⁺ = 0.038, H ₃ O ⁺ = 0.022	65	wet	66	5.1	144

^a Equilibrium concentrations presented. ^b Same as above.

TABLE 2. Summary of Particle Growth and Composition

expt	initial diameter ^a (nm)	final diameter (nm)	maximum seed mass ^b ($\mu\text{g}/\text{m}^3$)	maximum organic mass ^c ($\mu\text{g}/\text{m}^3$)	final organic mass/seed mass ^d ($\mu\text{g}/\mu\text{g}$)
1	127.8	339.1	1.38	4.75	15.8
2	201.7	409.1	2.94	6.51	7.9
3	248.1	507.5	5.00	16.97	13.4
4	258.1	478.1	4.61	9.95	12.0
5	232.7	232.7	11.70	0.96	0.13
6	289.4	522.6	10.40	39.46	12.4
7	231.7	440.1	7.1	39.88	10.3
8	248.1	478.1	na ^e	7.87	na
9	271.4	426.4	2.20	6.24	3.8
10	272.4	414.4	2.40	5.19	5.7

^a Aerodynamic diameter. ^b Loading of SO_4^{2-} only or NO_3^- only, at the end of the particle filling period. ^c Maximum observed glyoxal reaction product loading. This was typically observed soon after completion of the particle filling. ^d SO_4^{2-} or NO_3^- mass only. The ratio of organic to seed (SO_4^{2-} or NO_3^-) mass was computed at the end of the experiment. ^e The AMS is not sensitive to sea salt particles and hence a mass loading for the seed could not be obtained.

measure the evolving size distribution during the uptake of glyoxal (sampling mode). During the filling mode, polydisperse particles from the nebulizer were passed through a diffusion dryer and into the DMA where a single size was selected and introduced directly into the chamber. The diffusion dryer is not completely effective in drying the particles, and hence the initial state of the seed particles was wet in all cases except for experiment 5. To build up sufficient monodisperse particle mass in the chamber, the filling time was typically extended from 45 to 95 min. In the sampling mode, air from the chamber was drawn through the DMA, where particles were sized and counted by the CNC. A complete size distribution was acquired every 5 min.

Gaseous Glyoxal Generation and Measurement. Given the volatility of most carbonyl compounds, the preferred method of gas-phase introduction is to volatilize the liquid carbonyl in a heated stream of air or nitrogen. However, repeated attempts at producing gas-phase glyoxal in this manner were only marginally successful. This was primarily a result of the form of glyoxal in the commercially available 40 wt % aqueous solution. Glyoxal in this solution is rather nonvolatile and will not provide significant gas-phase levels in a 2 m³ chamber in a reasonable amount of time. Glyoxal is also known to polymerize at the temperatures needed for volatilization. As an alternative, solid glyoxal trimeric dihydrate (Aldrich) was dehydrated as described elsewhere (32) to yield gas-phase, monomeric glyoxal, which was flushed directly into the chamber via a stream of clean air. Once exposed to the interior Teflon surface, the glyoxal formed a visible film on this surface which continuously off-gassed glyoxal in the free monomeric form. This was not the desired result; however, measurement of gaseous glyoxal during each experiment revealed that the concentration remained relatively constant within the bag, indicating that equilibrium between the interior surface and the gas phase was quickly reached. This was fortuitous since it provided a near-constant gas-phase glyoxal concentration during each experiment, a condition most suitable for the present studies. Glyoxal concentrations were between 3.6 and 5.4 ppbv depending on the experiment. Gaseous glyoxal measurements were made on an automated version of a (2,4-dinitrophenyl)-hydrazine (2,4-DNPH) cartridge method coupled to an HPLC system equipped with a variable-wavelength UV absorbance detector (Hewlett-Packard). Glyoxal-DNPH was detected at 390 nm with a time resolution of 30 min. Aspects of this instrument have been described elsewhere (33).

Aerosol Mass Spectrometer Measurements. The particle composition was monitored with an Aerodyne aerosol mass spectrometer. Numerous publications have described the principle, operation, and applications of the AMS (34–37).

In brief, particles are sampled through a critical orifice and aerodynamic lens, which collimates the particles into a narrow beam and accelerates them into the time-of-flight region, ultimately impacting on a heater. A chopper is present, which may either completely block the particle beam or allow some material through at a defined frequency [time-of-flight (TOF) mode] or be completely open to allow all particles through [mass spectrum (MS) mode]. The velocity and hence size of the particle can be calculated from the time taken to reach the heater from the chopper. The particles are vaporized by the heater and subsequently ionized by electron impact (EI). The resulting ionized fragments are carried into a quadrupole mass spectrometer for detection. Each chamber in the AMS is differentially pumped, resulting in no discernible interference from trace gases. In the MS mode the mass spectrometer scans over a range of 1–300 amu, producing a mass spectrum that allows further quantification of mass for those species present in the particles. In the TOF mode the mass spectrometer is fixed on selected mass fragments that represent chemical species as a function of the time-of-flight, which allows for calculations of size-resolved distributions for these mass fragments. During these experiments, the AMS was operated in alternate MS–TOF mode, where each mode is active for several seconds. Quantification of an inorganic species such as $(\text{NH}_4)_2\text{SO}_4$ is based on the known fragmentation pattern and ionization efficiency (IE) relative to a calibration standard of NH_4NO_3 . Mass concentrations of inorganic and organic components were calculated on the basis of the principles given elsewhere (35). The AMS had a nominal inlet flow of ~ 1.4 cm³/s and operated continuously from the beginning of particle introduction into the chamber to a time before the bag was significantly depleted of air (1.5–4 h). The signal was averaged and a file was generated every 6 min.

Results and Discussion

Initial Particle Growth. Significant particle growth was observed during nearly all of the experiments that are summarized in Table 2. In many experiments the addition of organic mass doubled the particle diameter in a short period of time and resulted in a primarily organic particle. In general, the shapes of the time-dependent mass loading curves were the same for all experiments (Figure 2). Once the particles were exposed to preexisting gaseous glyoxal in the chamber, growth was observed immediately and hence the organic and sulfate mass increase simultaneously from the beginning of the experiment. Blank experiments demonstrated that there was no particle growth in the absence of glyoxal and negligible organic mass.

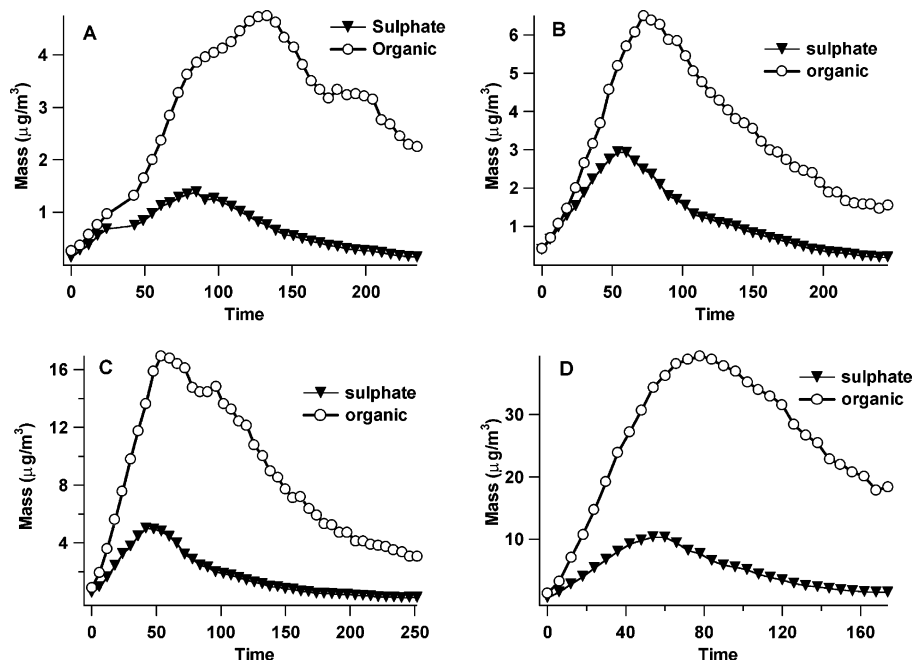


FIGURE 2. Time-dependent mass loading of particulate sulfate and organics for selected experiments. Organics corresponds to the sum of all glyoxal reaction products present. (A) Experiment 1; (B) experiment 2; (C) experiment 3; (D) experiment 6.

Wall Loss. The maximum in the loading of SO_4^{2-} corresponds to the end of particle filling, at which point the observed decrease in mass is attributed to ongoing particle wall losses, confirmed by the DMA/CNC system. Although wall losses decrease the total particle number, the mass of sulfate on a per-particle basis should remain constant upon completion of filling, for all experiments. This was verified by calculating the ratio of the sulfate loading (micrograms per cubic meter) derived from the AMS to the number concentration obtained simultaneously from the DMA/CNC. This ratio as a function of time is shown in Figure 3A and was found to be constant for these experiments within the experimental error (typically 5–20% RSD).

Glyoxal Uptake on Aerosols. Since the amount of SO_4^{2-} within individual particles was constant throughout a given experiment, normalizing the organic mass to the sulfate mass can remove the effects of wall losses and is a meaningful representation of the extent of glyoxal uptake. This ratio is shown in Figure 3B for selected experiments. As the figure shows, the organic/seed mass ratio typically increases continuously throughout the experiments, indicating that an equilibrium is not reached. The curves show evidence of positive curvature, indicating that the rate of glyoxal uptake on a per-particle basis actually increases throughout an experiment. This is likely attributable to the increased surface area of the particles as they grow. A detailed quantitative analysis of the resultant uptake coefficients, γ , derived from a fit of the growth data to a mathematical model, is described elsewhere (38). Qualitatively, however, the uptake of glyoxal was independent of seed type, given that significant increases in organic mass were observed for particles of pure ammonium sulfate, ammonium sulfate/sulfuric acid mixtures, simulated sea salt, and sodium nitrate.

Effect of Relative Humidity and Acidity on Uptake. A significant effect on organic growth was observed by varying the relative humidity. At very low RH (experiment 5) there was no discernible particle growth and limited organic mass was detected. Conversely, increasing the RH (experiment 3) to greater than 50% dramatically increased the organic mass observed. However, further increasing the RH to greater than 80% (experiment 4) tended to slightly reduce the organic mass, which is reflected in the ratio of organic to seed mass in Table 2.

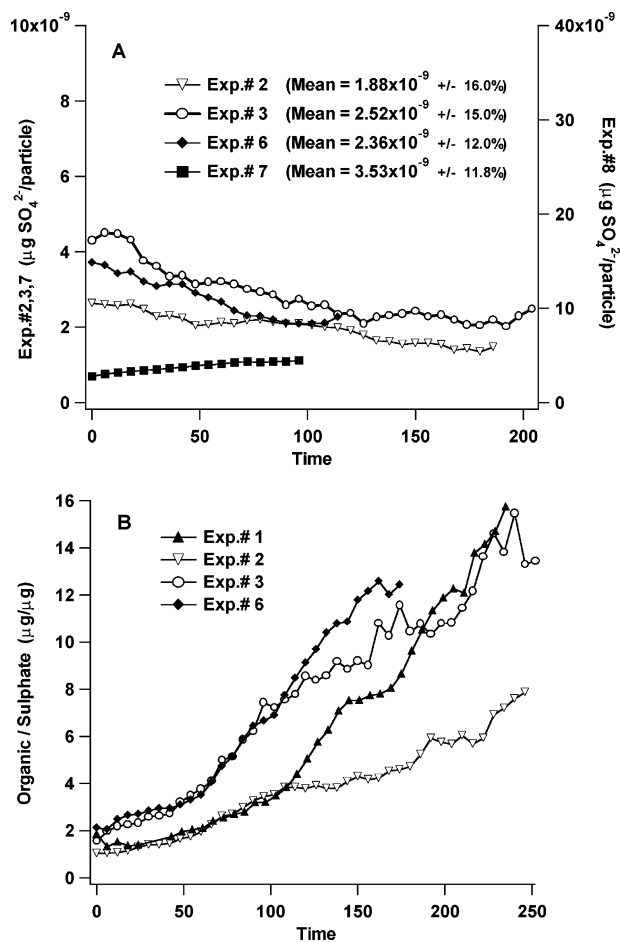
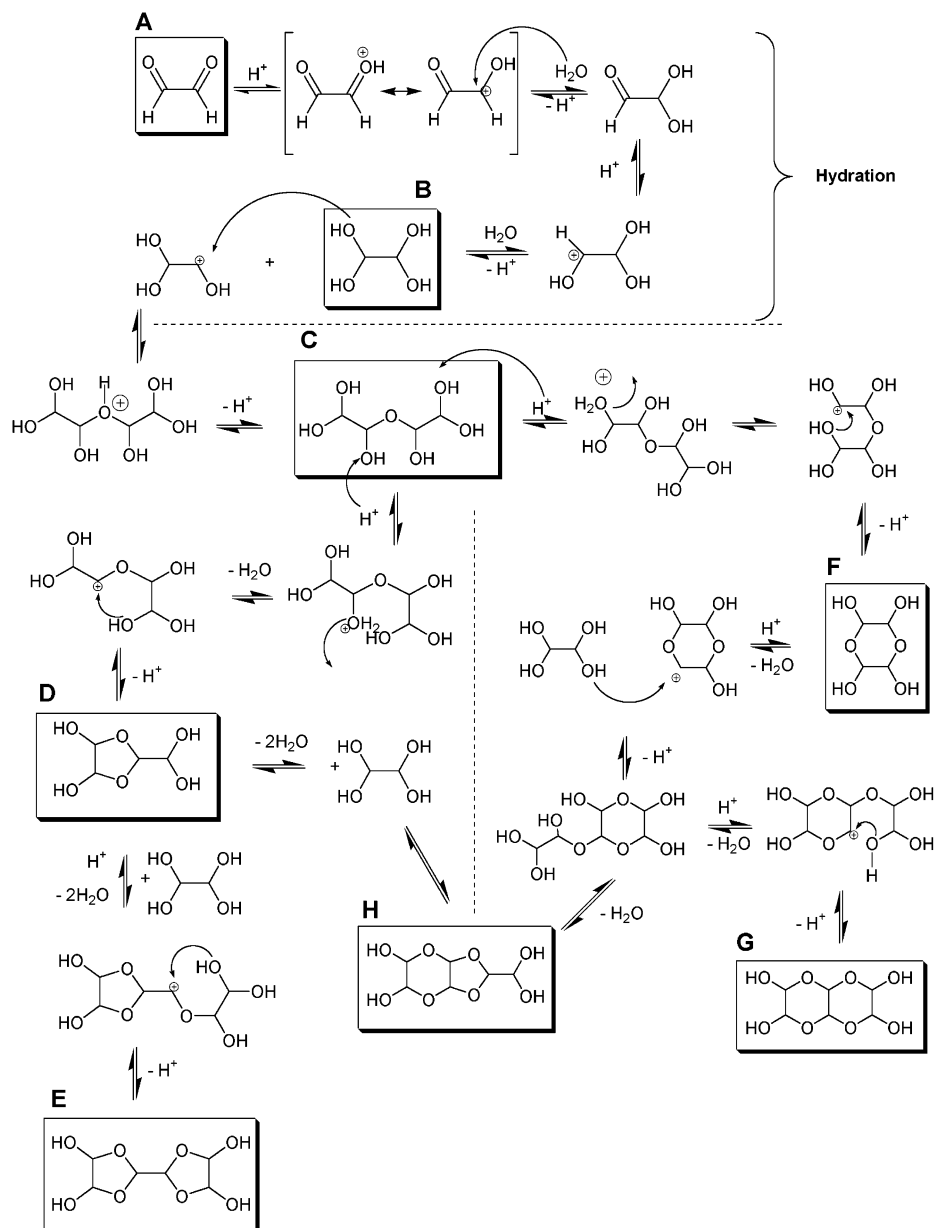


FIGURE 3. (A) Sulfate mass on a per-particle basis as a function of time for selected experiments. (B) Ratio of organic mass to sulfate mass as a function of time for selected experiments, as determined by the AMS.

The effect of particle acidity on the glyoxal uptake is less pronounced than that of RH, although for a given RH and seed type, significantly increasing the acid concentration

SCHEME 1. Potential Mechanism for the Uptake and Subsequent Reaction of Glyoxal in Particulate Matter



(experiments 1 and 6, and 2 and 7) generally tends to increase the reactive uptake of glyoxal, as indicated by the maximum organic mass observed during an experiment. To be consistent with the observed trends, a proposed mechanism must be strongly dependent on the particulate water concentration and likely acid-catalyzed. Figure 3B shows that the organic mass on the particles continuously increased during each experiment, implying that, at least on the time scale of these experiments, a steady state between gas-phase glyoxal and the uptake products was not reached. This suggests that a reaction or series of reactions may be occurring in the aerosols that is irreversible under these conditions, leading to products with low vapor pressures.

Reaction Mechanism. A reaction mechanism specific to glyoxal to explain the observed uptake is given in Scheme 1, based on generic hydration and acetal formation mechanisms that have been studied previously (20, 22). The first step invariably involves the dissolution of gaseous glyoxal (A) into the available aqueous phase of the particulate matter, and subsequent hydration forming a geminal diol (B). Protonation and reaction of two geminal diol molecules results in the

formation of an acetal (C), which is likely to undergo further dehydration, forming a more stable five-membered ring structure (D). Additional dehydration can also occur, resulting in structure E, containing three hydrated glyoxal units. At this point further protonation and dehydration is unlikely except under highly acidic conditions. The analogous formation of six-membered ring structures F and G is also possible, as well as structure H. The entire process as written can be acid-catalyzed. Although either mechanism is plausible ($\text{C} \rightarrow \text{D} \rightarrow \text{E}$ or $\text{C} \rightarrow \text{F} \rightarrow \text{G}$), it has been shown that the dominant forms of glyoxal in aqueous solutions between 1 and 10 M are primarily D and E (39–41), likely a result of the free rotation of the central C–C bond in these structures as compared to the rigid structures of F and G. The *gem*-diol form (B) dominates (>90%) in dilute solutions less than 1 M. Higher order oligomers are thought only to arise in highly concentrated glyoxal solutions (39–41). The vapor pressures of the active compounds in aqueous solutions (structures D and E) have been estimated at less than 1×10^{-5} kPa (IUCALD data set), sufficiently low enough for the compounds to remain in the condensed phase. The particle mass spectral

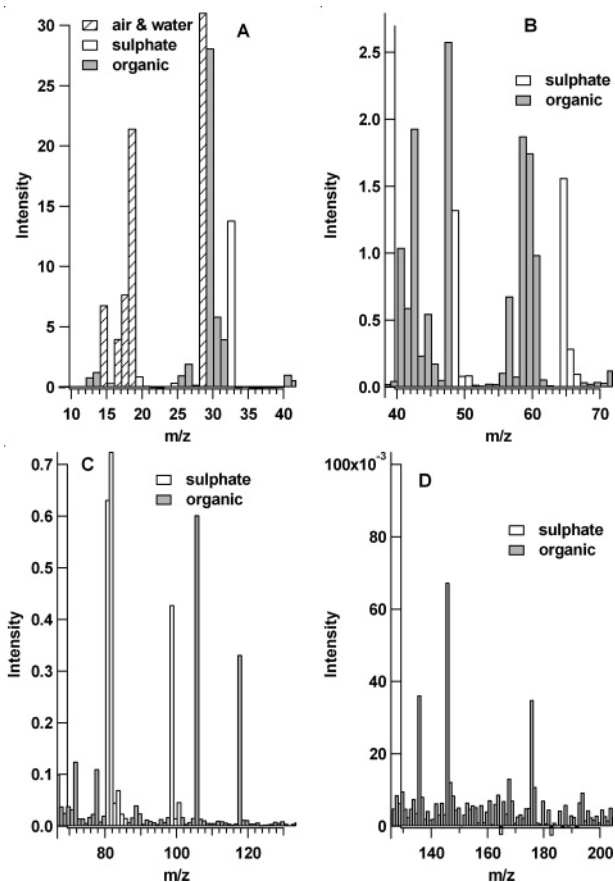


FIGURE 4. Sample particle mass spectra obtained from experiment 6: (A) m/z 10–40; (B) m/z 40–70; (C) m/z 70–130; (D) m/z 130–200.

results from the present experiments support many aspects of the proposed mechanism in Scheme 1.

A sample particle mass spectrum and tentative organic fragment identification is given in Figure 4 and Table 3. Several fragments that can only arise from a glyoxal oligomer have been identified (m/z 88, 105, 117, 135, 192, and 193)

from the mass spectrum. These fragments typically have relative intensities of less than 2% but are clearly observable above the background. The low relative intensities for these fragments do not indicate that oligomeric forms of glyoxal are insignificant. It is more likely that these forms are thermally unstable at the vaporization temperature of the AMS (500 °C), and readily revert to the monomer or *gem*-diol form before entering the ionization region. As a result, the intensity of small fragments (m/z 29, 30, 31, and 58) may be enhanced. A second possibility exists, whereby structures D and E yield these low mass fragments directly as major products during ionization. Without reference spectra for the pure compounds, it is not possible to ascertain the contribution from each oligomer in a given mass spectrum. Further complicating the mass spectral interpretation is the fact that compounds of this type do not yield an observable parent ion (M^+) (42–44), and many larger fragments can arise from both structures D and E. However, fragments with an m/z of 192 and 193 are unlikely to arise from structures other than E or higher order oligomers, which confirm that two or more dehydration reactions as depicted in Scheme 1 must have occurred.

The time evolution of m/z 193 and other important fragments for a selected experiment is given in Figure 5. A delay in the appearance of larger mass fragments such as 193 indicates that several species are present and that the rate of formation for larger oligomers is slower than that for the *gem*-diol or structure D. Similarly, m/z 135 is likely also from a higher order product given its delayed increase relative to sulfate and the smaller fragments. Given that hydration is likely a fast process, ions with an initial time evolution closely matching that of a SO_4^{2-} fragment (m/z 48) likely arise primarily from the hydrated monomer (i.e., m/z 47). This also explains the rapid particle growth that occurred when the seed aerosols were introduced into the gaseous glyoxal (Figure 2). Other ions of intermediate size have a time evolution somewhere between that of m/z 48 (SO_4^{2-} fragment) and m/z 193 (structure E). These fragments may arise from more than a single species, and their time evolution is dependent upon a combination of the fragmentation of each oligomer and the time evolution of the abundance of the oligomer.

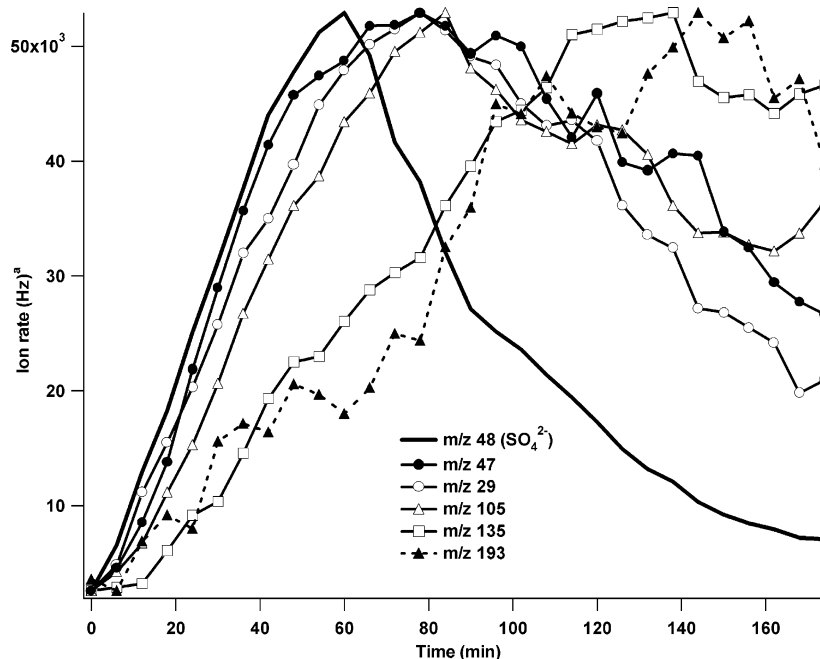


FIGURE 5. Typical time evolution of selected ions. ^aOnly the ion rate for m/z 48 is shown. All others have been normalized to this ion rate for clarity purposes.

TABLE 3. Tentative Structure Identification of Selected Ions from the Particle Mass Spectra of Experiment 7

<i>m/z</i>	Relative Intensity ^a (%)	Tentative fragment structure ^b	Potential Origin
29	100	CHO or COH	A-G
30	21	CHOH	A-G
47	9		B,D
60	3.5		B,D,E
77	0.4		B,D,E
105	2		D,E
135	0.1		D,E
117	1.2		D,E
118	0.05		D,E
192	0.025		E
193	0.03		E

^a Intensity relative to the largest ions known to originate from the organic mass. ^b Other isomers for many of these ions are possible. The exact structure for those ions that have lost water is not known. The location of the positive charge is not shown.

The effect of RH on the time evolution of selected ions is shown in Figure 6. At low RH (25%) the onset of most organic ions in the mass spectrum, particularly those with a low *m/z*, closely matches the onset of the SO₄²⁻ ion (*m/z* 48). Larger ions, which cannot be formed from the *gem*-diol, are only slightly shifted. Increasing the RH significantly slows the evolution of all observed organic ions relative to *m/z* 48. This is consistent with the proposed chemical mechanism, under the condition that gas-phase diffusion to the particle surface is the limiting step in the hydration of glyoxal. It may also imply that the mechanism is acid-catalyzed, given that dilution decreases particle acidity. These aspects are discussed in more detail in a subsequent paper (38). Increasing the relative humidity would increase the amount of water within the particles, effectively diluting the hydrated glyoxal (in a diffusion-limited process). Since the rate of formation of oligomers, as written in Scheme 1, is proportional to the concentration of the *gem*-diol, dilution is expected to slow oligomer formation. Conversely, the rate of hydration should not decrease with increasing particulate water content, and hence the evolution of those fragments arising largely from the *gem*-diol should not be delayed as much as the larger fragments. The fact that the onset of all organic fragments was delayed relative to *m/z* 48 to some degree implies that

several species (including the hydrated glyoxal) were present and that the formation of at least some of the contributing species was delayed upon dilution at higher RH. Thus their relative contributions to the organic particle mass are significantly dependent on the available particulate water.

Significant fragments with an *m/z* ratio higher than 193 or with a slower time evolution were not detected. Although this may indicate that only compounds B, D, and E were present in the particulate matter, it is also possible that decomposition of higher order products in the vaporization region of the AMS occurred. Thus the contribution of individual species to the overall particle composition cannot be determined. One can only conclude that several reactions occurred simultaneously and that the proposed mechanism is consistent with the observed mass spectra.

Glyoxal Sulfates. Analysis of the particle mass spectrum (Figure 4) revealed two significant fragments (*m/z* 175 and 145) that could not be identified with structures from the proposed mechanism. A mass fragment of 175 would require a loss of mass 35 from structure E, which cannot be formulated even with several unimolecular fragmentation steps. Higher order glyoxal oligomers fashioned in the same manner as in Scheme 1 would likely fragment in a manner similar to structures D and E and also would not yield a mass

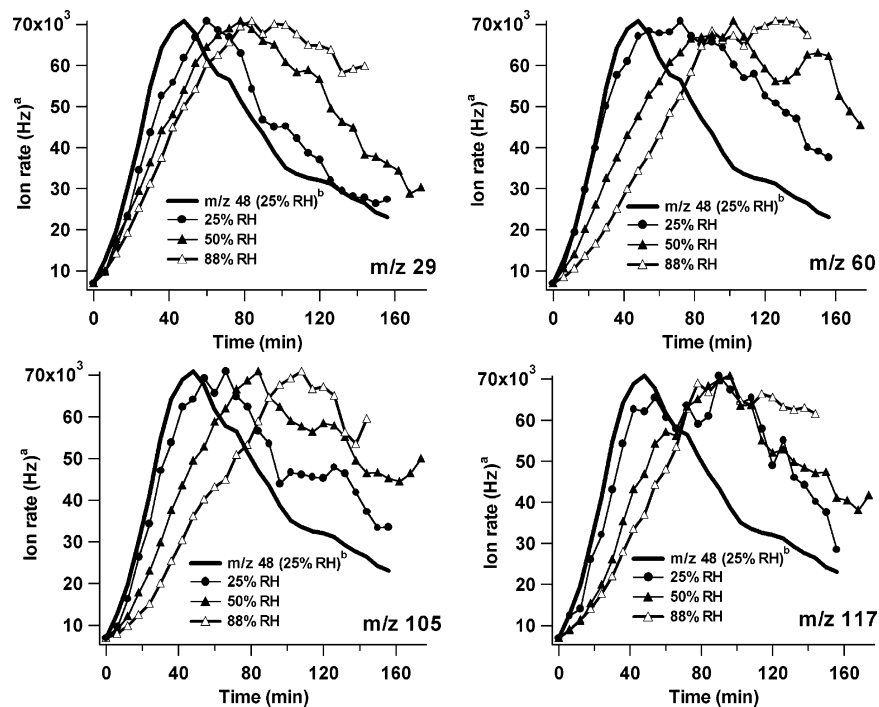


FIGURE 6. Effect of relative humidity on the time evolution of selected ions for experiments of constant acidified seed type; nitrogen/sulfur ratio = 0.36 (experiments 6 and 7 and experiment at RH = 25%; not shown in Tables 1 and 2). Key: ^aOnly the ion rate for *m/z* 48 is shown. All others are normalized to this ion rate for clarity purposes. ^bTime evolution of the sulfate mass (*m/z* 48) is shown at 25% RH only, since it is insensitive to changes in RH.

of 175. However, the sulfate esterification mechanism proposed in Scheme 2 can form products that are able to generate fragments 145 and 175. Esterification of alcohols by sulfuric acid or bisulfate has long been known to occur at room temperature in bulk solution (45–47) and has been hypothesized as one possible mechanism for irreversible uptake of hydrated formaldehyde on aqueous acidic surfaces (48). Hydrated glyoxal, with four alcohol functional groups, is likely even more susceptible to such a reaction. In Scheme 2 glyoxal is first hydrated and protonated, followed by reaction with any of the three sulfate species present. Subsequent loss or gain of a proton results in neutral compound C_2 with a mass of 174. The observed *m/z* of 175 arises from the addition of a proton to any one of the oxygen atoms yielding the $M + 1$ ion. Although a negligible $M + 1$ signal was observed for oligomers of glyoxal in Scheme 1, organic sulfates are known to produce significant enhancements of the $M + 1$ ion, even in low-pressure conditions, which has been attributed to the high number of basic centers present in the sulfate (49). The $M + 1$ ion is always observable from organic sulfates and can have a relative abundance of greater than 5% for some molecules (49).

Another typical fragmentation for organic sulfates is a hydrogen loss, followed by the subsequent rearrangement of the ion and loss of CO (49). Applying this fragmentation to glyoxal sulfate (structure C_2) can result in the observed 145 ion ($M^+ - 1 - 28 = 145$). However, virtually all other important ions that are likely to form from C_2 are indistinguishable from fragments formed by any glyoxal oligomer in Scheme 1 and from sulfate fragments. It was expected that a major ion would be produced from the loss of SO_3 from the $M - 1$ ion (49), yielding a mass of 93, and although this ion was observed, it can also be formed via the loss of a hydrogen from the hydrated glyoxal. Other important fragments expected from this organic sulfate include 80, 81, 82, and 98, but they were overwhelmed by the fragmentation of sulfate, bisulfate, or sulfuric acid in the seed aerosols. Cyclization of C_2 analogous to the cyclization in Scheme 1

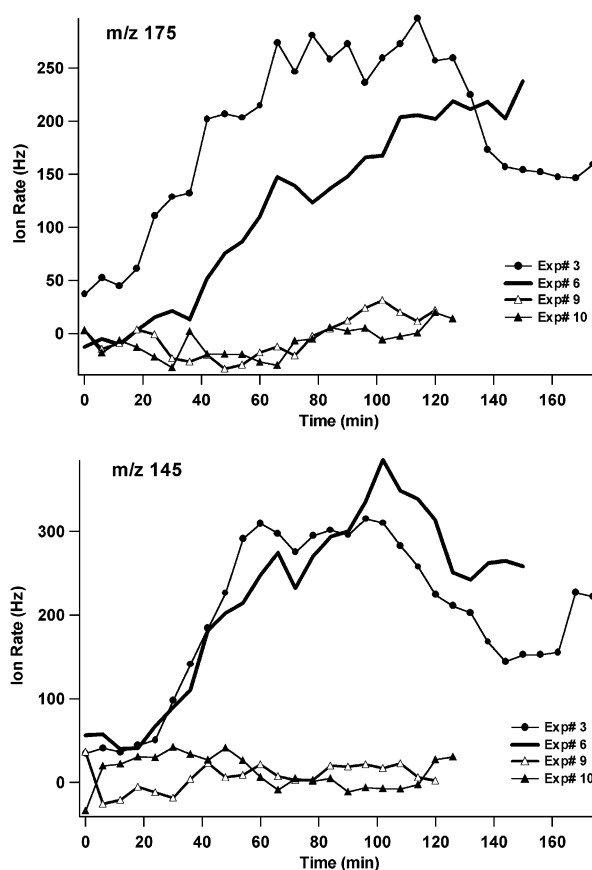
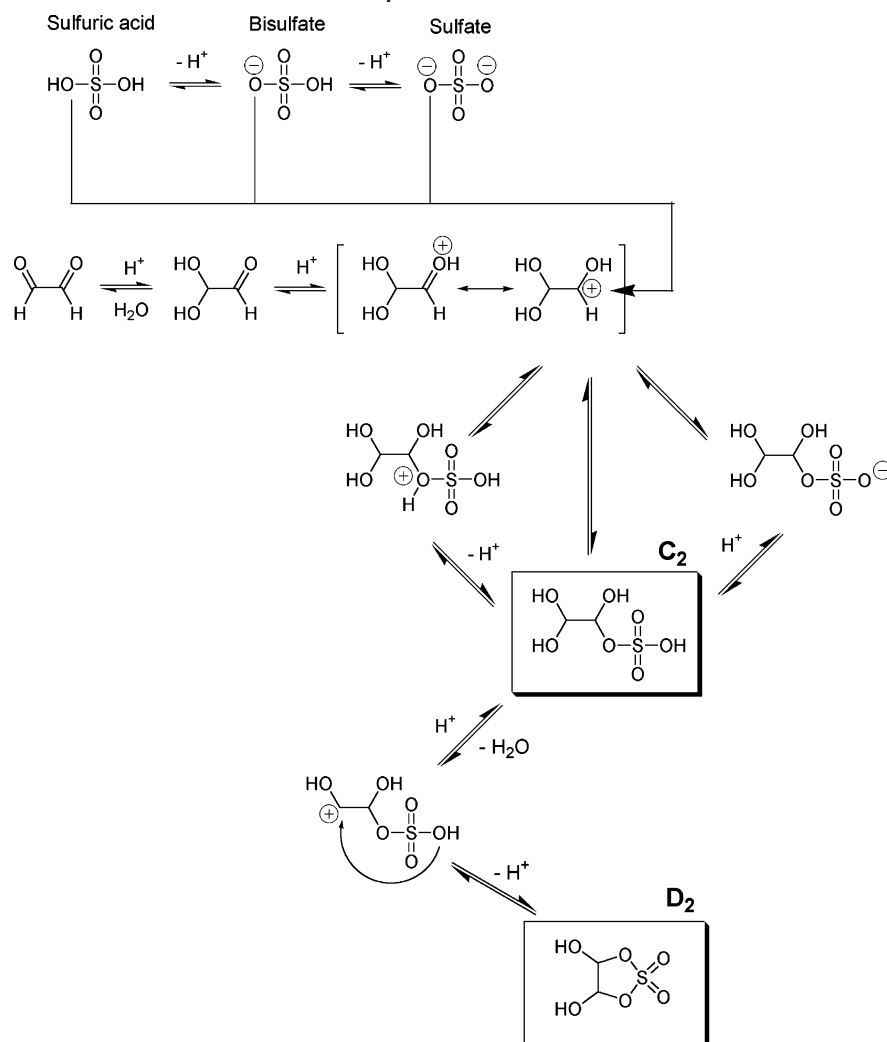


FIGURE 7. Time evolution of ions attributed to glyoxal sulfates, for experiments using sulfate-containing particles (experiments 3 and 6) and nonsulfate particles (NaCl, experiment 8, and $NaNO_3$, experiment 9). The intensity of these ions in experiment 10 was also approximately 0 but is not shown here for clarity purposes.

SCHEME 2. Proposed Mechanism for the Formation of Glyoxal Sulfates in Particulate Matter



can also yield structure D_2 , but no unique fragments from this structure with a significant intensity were detected. Other structural possibilities besides C_2 and D_2 that contain sulfates cannot be ruled out.

Additional evidence for the formation of glyoxal sulfates is presented in Figure 7. If an organic sulfate was formed, then this reaction must not proceed on particles other than those containing sulfur species. Experiments 8, 9, and 10 were conducted with NaCl and NaNO_3 particles. It is clear that the signal intensity for fragments 145 and 175 was approximately zero within experimental error for these nonsulfate seed aerosols, while fragments associated with oligomers from Scheme 1 were present.

The contribution of these organic sulfates to the total organic mass of the particles cannot be determined since these compounds are also likely thermally unstable at the vaporization temperature used here, and a reference mass spectrum for the pure compound is unavailable. The relevance of the formation of organic sulfates in ambient particulate matter is therefore uncertain. However, given that several of these experiments were performed under conditions similar to or within the range of conditions seen in the real atmosphere (a low initial aerosol seed mass loading, 50% relative humidity, and ppb levels of glyoxal), it is reasonable to expect these reactions to occur in ambient aerosols as a means of glyoxal uptake. Other carbonyl compounds may also react similarly, suggesting that the contribution of all carbonyl compounds to SOA formation

may be significant. In addition, it is highly likely that, given the multitude of carbonyl compounds that exist in the atmosphere, cross-condensation or acetal formation reactions to form complicated polymeric structures in the particles would be a more important process that self-reactions for each carbonyl species. Organic sulfate formation is potentially equally as important as any hydration/acetal formation mechanism, although the relative significance of each mechanism to atmospheric aerosols is unclear. To the best of our knowledge, this is the first observation of heterogeneous organic sulfate formation in particulate matter. Measurement of the various heterogeneous products in ambient particulate matter is a logical progression in order to assess the true relevance of these reactions.

Acknowledgments

We acknowledge the National Science and Engineering Research Council and the Meteorological Service of Canada for funding. We thank Dr. Richard Leaitch and Kathy Hayden for technical support with the AMS. We acknowledge Michael Mozurkewich and Tak Wai Chan for use of and technical support with the DMA/CNC. Finally we thank the reviewers of this paper, who provided invaluable comments.

Literature Cited

- (1) Twomey, S. Aerosols, clouds and radiation. *Atmos. Environ.* **1991**, 25A (11), 2435–2442.

- (2) Pilinis, C.; Pandis, S. N.; Seinfeld, J. H. Sensitivity of direct climate forcing by atmospheric aerosols to aerosol size and composition. *J. Geophys. Res.* **1995**, *100*, 18739–18754.
- (3) Eldering, A.; Cass, G. R. Source-oriented model for air pollutant effects on visibility. *J. Geophys. Res.* **1996**, *101*, 19343–19369.
- (4) Eldering, A.; et al. Development of an improved image processing based visibility model. *Environ. Sci. Technol.* **1993**, *27*, 626–35.
- (5) Yuan, C. S.; Lee, C. G.; Chang, J. C.; Liu, S. H.; Yuan, C.; Yang, H. Y. Correlation of atmospheric visibility with chemical composition and size distribution of aerosol particles in urban area. *Proceedings of the AWMA 93rd Annual Meeting*; Air and Waste Management Association: 2000; paper 87, pp 1–18.
- (6) *Air Quality Criteria for Particulate Matter*; Environmental Protection Agency: Washington, DC, 1996; p 95.
- (7) Dockery, D. W.; et al. An association between air pollution and mortality in six U.S. cities. *N. Engl. J. Med.* **1993**, *329* (24), 1753–9.
- (8) Schwartz, J.; Dockery, D. W. Particulate air pollution and daily mortality in Steubenville, Ohio. *Am. J. Epidemiol.* **1992**, *135*, 12–9.
- (9) Bowman, F. M.; et al. Mathematical model for gas-particle partitioning of secondary organic aerosols. *Atmos. Environ.* **1997**, *31*, 3921–3931.
- (10) Pankow, J. F. Review and comparative analysis of the theories on partitioning between the gas and aerosol particulate phases in the atmosphere. *Atmos. Environ.* **1987**, *21*, 2275–2283.
- (11) Pankow, J. F. An absorption model of the gas/aerosol partitioning involved in the formation of secondary organic aerosol. *Atmos. Environ.* **1994**, *28*, 189–193.
- (12) Pankow, J. F. An absorption model of gas/particle partitioning of organic compounds in the atmosphere. *Atmos. Environ.* **1994**, *28* (2), 185–188.
- (13) Jang, M.; Kamens, R. M. Characterization of secondary aerosol from the photooxidation of toluene in the presence of NO_x and 1-propene. *Environ. Sci. Technol.* **2001**, *35* (18), 3626–3639.
- (14) Kamens, R. M.; Jaoui, M. Modeling aerosol formation from alpha-pinene + NO_x in the presence of natural sunlight using gas-phase kinetics and gas-particle partitioning theory. *Environ. Sci. Technol.* **2001**, *35* (7), 1394–405.
- (15) Seinfeld, J. H.; Pandis, S. *Atmospheric Chemistry and Physics: From Air Pollution to Climate Change*; John Wiley & Sons: New York, 1998.
- (16) Noziere, B.; Barnes, I.; Becker, K.-H. Product study and mechanisms of the reactions of α -pinene and of pinonaldehyde with OH radicals. *J. Geophys. Res.* **1999**, *104* (D19), 23645–23656.
- (17) Grosjean, E.; Grosjean, D.; Seinfeld, J. H. Atmospheric chemistry of 1-octene, 1-decene, and cyclohexene: gas-phase carbonyl and peroxyacyl nitrate products. *Environ. Sci. Technol.* **1996**, *30* (3), 1038–47.
- (18) Olson, T. M.; Hoffmann, M. R. Hydroxyalkylsulfonate formation: its role as a sulfur (IV) reservoir in atmospheric water droplets. *Atmos. Environ.* **1989**, *23* (5), 985–97.
- (19) Tobias, H. J.; Ziemann, P. J. Thermal desorption mass spectrometric analysis of organic aerosol formed from reactions of 1-tetradecene and O₃ in the presence of alcohols and carboxylic acids. *Environ. Sci. Technol.* **2000**, *34* (11), 2105–2115.
- (20) Jang, M.; et al. Particle growth by acid-catalyzed heterogeneous reactions of organic carbonyls on preexisting aerosols. *Environ. Sci. Technol.* **2003**, *37* (17), 3828–37.
- (21) Jang, M.; et al. Heterogeneous atmospheric aerosol production by acid-catalyzed particle-phase reactions. *Science* **2002**, *298*, 814–817.
- (22) Jang, M.; Kamens, R. M. Atmospheric secondary aerosol formation by heterogeneous reactions of aldehydes in the presence of a sulfuric acid aerosol catalyst. *Environ. Sci. Technol.* **2001**, *35* (24), 4758–66.
- (23) Noziere, B.; Riemer, D. D. The chemical processing of gas-phase carbonyl compounds by sulfuric acid aerosols: 2,4-pentandione. *Atmos. Environ.* **2003**, *37*, 841–851.
- (24) Tuazon, E. C.; et al. Yields of glyoxal and methylglyoxal from the NO_x-Air photooxidations of toluene and *m*- and *p*-xylene. *Environ. Sci. Technol.* **1984**, *18* (12), 981–984.
- (25) Bandow, H.; Washida, N. Ring-cleavage reactions of aromatic hydrocarbons studied by FTIR spectroscopy. II. Photooxidation of *o*-, *m*-, and *p*-xylenes in the NO_x-air system. *Bull. Chem. Soc. Jpn.* **1985**, *58* (9), 2541–2548.
- (26) Bandow, H.; Washida, N.; Akimoto, H. Ring-cleavage reactions of aromatic hydrocarbons studied by FTIR spectroscopy. I. Photooxidation of toluene and benzene in the NO_x-air system. *Bull. Chem. Soc. Jpn.* **1985**, *58* (9), 2531–2540.
- (27) Yu, J.; Jeffries, H. E.; Sexton, K. G. Atmospheric photooxidation of alkylbenzenes I. Carbonyl product analyses. *Atmos. Environ.* **1997**, *31* (15), 2261–2280.
- (28) Yu, J.; Jeffries, H. E.; Le Lacheur, R. M. Identifying airborne carbonyl compounds in isoprene atmospheric photooxidation products by their PFBHA oximes using gas chromatography/ion trap mass spectrometry. *Environ. Sci. Technol.* **1995**, *29* (8), 1923–32.
- (29) Stevens, P. S.; Seymour, E.; Li, Z. Theoretical and experimental studies of the reaction of OH with isoprene. *J. Phys. Chem. A* **2000**, *104* (25), 5989–5997.
- (30) Carter, W. P. L.; Atkinson, R. Development and evaluation of a detailed mechanism for the atmospheric reactions of isoprene and NO_x. *Int. J. Chem. Kinet.* **1996**, *28* (7), 497–530.
- (31) Fick, J.; et al. Effect of OH radicals, relative humidity, and time on the composition of the products formed in the ozonolysis of α -pinene. *Atmos. Environ.* **2003**, *37* (29), 4087–4096.
- (32) Steacie, E. W. R.; Hatcher, W. H.; Horwood, J. F. Kinetics of the decomposition of gaseous glyoxal. *J. Chem. Phys.* **1935**, *3*, 291–5.
- (33) Aiello, M. An automated instrument for the quantitation of atmospheric carbonyls: measurements and interpretation in southern Ontario. Ph.D. Thesis, York University, Toronto, Canada, 2004.
- (34) Allan, J. D.; et al. Quantitative sampling using an aerodyne aerosol mass spectrometer 2. measurements of fine particulate chemical composition in two U.K. cities. *J. Geophys. Res.* **2003**, *108* (D3), 4091.
- (35) Allan, J. D., et al., Quantitative sampling using an Aerodyne aerosol mass spectrometer 1. techniques of data interpretation and error analysis. *J. Geophys. Res.* **2003**, *108* (D3), 4090.
- (36) Jayne, J. T. Development of an aerosol mass spectrometer for size and composition analysis of submicron particles. *Aerosol Sci. Technol.* **2000**, *33*, 49–70.
- (37) Jimenez, J. L.; et al. Ambient aerosol sampling using the Aerodyne aerosol mass spectrometer. *J. Geophys. Res.* **2003**, *108* (D7), SOS 13/1–13/13.
- (38) Liggio, J.; Li, S.-M.; McLaren, R. Reactive uptake of glyoxal to atmospheric particulate matter. *J. Geophys. Res.* (in press).
- (39) Fratzke, A. R.; Reilly, P. J. Thermodynamic and kinetic analysis of the dimerization of aqueous glyoxal. *Int. J. Chem. Kinet.* **1986**, *18* (7), 775–89.
- (40) Fratzke, A. R.; Reilly, P. J. Kinetic analysis of the disproportionation of aqueous glyoxal. *Int. J. Chem. Kinet.* **1986**, *18* (7), 757–73.
- (41) Whipple, E. B. Structure of glyoxal in water. *J. Am. Chem. Soc.* **1970**, *92*, 2 (24), 7183–6.
- (42) Beynon, J. H.; Saunders, R. A.; Williams, A. E. *The Mass Spectra of Organic Molecules*; Elsevier Publishing Co.: Amsterdam, 1968; Vol. IX, p 511.
- (43) Porter, Q. N.; Baldas, J. *Mass Spectrometry of Heterocyclic Compounds*; Wiley-Interscience: New York, 1971; Vol. XVII, p 564.
- (44) Hamming, M. C.; Foster, N. G. *Interpretation of Mass Spectra of Organic Compounds*; Academic Press: New York, 1972; Vol. XIV, p 694.
- (45) Garner, H. K.; Lucas, H. J. Preparation and hydrolysis of some acetals and esters of D(-)-2,3-butanediol. *J. Am. Chem. Soc.* **1950**, *72*, 5497–5501.
- (46) Deno, N. C.; Newman, M. S. Mechanism of sulfation of alcohols. *J. Am. Chem. Soc.* **1950**, *72*, 3852–56.
- (47) Clark, D. J.; Williams, G. Esterification by sulfuric acid II, Ethyl alcohol. *J. Chem. Soc.* **1957**, 4218–4221.
- (48) Iraci, L. T.; Tolbert, M. A. Heterogeneous interaction of formaldehyde with cold sulfuric acid: implications for the upper troposphere and lower stratosphere. *J. Geophys. Res.* **1997**, *102* (D13), 16099–107.
- (49) Lloyd, E. J.; Porter, Q. N. Mass spectrometric studies. XII. Organic sulfates. *Aust. J. Chem.* **1977**, *30* (3), 569–78.

Received for review February 18, 2004. Revised manuscript received October 18, 2004. Accepted November 11, 2004.

ES048375Y